

ANALYTIC AND NUMERICAL STUDIES OF THE MODIFIED BETATRON

T. P. Hughes, M. M. Campbell and B. B. Godfrey  
 Mission Research Corporation  
 1720 Randolph Road, S.E.  
 Albuquerque, New Mexico 87106

SUMMARY

The modified betatron concept<sup>1,2</sup> has been proposed as a means of accelerating high current (kilo-amp) electron beams to high energy. This device employs a toroidal magnetic field to overcome the space-charge limit on the current in a conventional betatron<sup>3</sup> at low energy. In this paper, we look at the injection, equilibrium and stability of the modified betatron. The main emphasis is on stability. An analytic dispersion relation is derived using a cold-fluid model of the beam. The results are compared to three-dimensional simulations performed with the electromagnetic PIC code IVORY.<sup>4</sup> The nonlinear development of the negative mass instability is followed in the simulations.

BEAM INJECTION

In the modified betatron, the equilibrium radial location of the beam centroid is determined by equating the centrifugal force to the opposing  $v \times B$  force from the self and applied vertical field  $B_z$ . Kapetanacos, et. al<sup>5</sup> have shown that under certain conditions there is a fortunate cancellation of two effects, and the equilibrium radius is given simply by  $r_0 = \gamma_0 \beta m c / e B_{z0}$  where  $e$  and  $m$  are the electron charge and mass respectively,  $B_{z0}$  is the applied vertical magnetic field,  $\gamma_0 m c^2$  is the injected electron energy and  $\beta = (1 - 1/\gamma_0^2)^{1/2}$ . This result is confirmed by a 3-D IVORY simulation in which a pulse was injected into a 1 m radius torus. The coordinate system for this and all the other results we report is cylindrical,  $r, \theta, z$ , where the  $z$ -axis coincides with the major axis of the torus, and  $\theta$  is the toroidal coordinate. The pulse has a finite rise and fall-time in current  $I$  and energy  $\gamma$ , with  $I = 0$  to 10 kA,  $\gamma = 2$  to 5 over 5 ns in the head, followed by a 10 ns "body" with  $I = 10$  kA,  $\gamma = 5$ , and finally a 5 ns tail mirroring the head. These values for  $\gamma$  are the space-charge depressed values attained inside the drift region. The injection energy  $\gamma_0$  has somewhat larger values:  $\gamma_0 = 7$  in the "body" of the beam. The vertical field applied was  $B_z = 114$  gauss, which, when combined with  $\gamma_0$ , gives an equilibrium radius of 102 cm. The body of the pulse in fact propagates quiescently through the first turn (which is as far as the simulation ran) at about this radius. A snapshot of the beam near the end of injection is shown in Fig. 1. The lack of radial force balance in the head (and tail) of the beam due to the lower value of  $\gamma$  causes an  $F \times B_\theta$  drift in the  $z$  direction. The resulting deposition of energy on the wall may create plasma, leading to vacuum degradation and possibly an ion resonance instability of the beam.<sup>6</sup> We have also simulated a case where the beam is injected with a radial offset of 4 cm from the center of the drift tube. The results showed similar good behavior on the first turn.

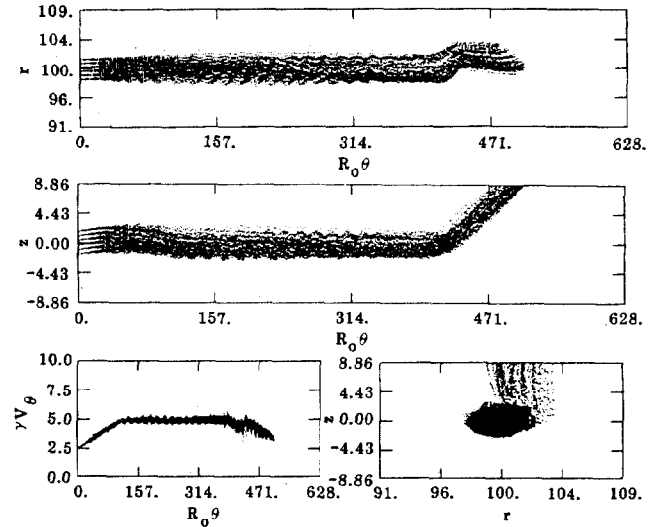


Figure 1. Phase space plots of a 20 ns beam pulse being injected at  $\theta=0, r=R=100$  cm,  $z=0$  into a betatron. While the upper two plots are rectangular, the simulation was done in toroidal geometry. Lengths are in cm;  $v/c$  is normalized to  $c$ .

BEAM EQUILIBRIUM

If the acceleration time in a 1 m radius betatron is 1 millisecond, the beam rotates about 48,000 times during the acceleration. It is therefore essential to have accessible self-consistent equilibria for the beam. In analytic and numerical work, such equilibria form the starting point for study of beam stability. Using a cold-fluid model of the beam, Finn and Manheimer<sup>7</sup> have shown that self-consistent equilibria do in fact exist. We have used Finn's code EQUIL3<sup>8</sup> to initialize IVORY with a 10 kA beam at  $\gamma_0 = 14$ . The noise present in IVORY due to discrete particle effects cause deviations from the perfect laminarity assumed in EQUIL3. IVORY simulations therefore provide a test of the sensitivity of the equilibria to the cold-fluid assumption. In our simulations, we propagated the beam for twenty revolutions around the torus during which time the beam rotated twice about its own axis. No off-centering drifts were observed, and the beam minor radius remained constant. From this it appears that the EQUIL3 equilibria are not greatly affected by the addition of small amounts of temperature. The methods of Finn and Manheimer break down as the transition from diamagnetic to paramagnetic rotation of the beam about its own axis is approached.<sup>7</sup> An interesting, though perhaps lengthy, simulation would be to take one of their diamagnetic equilibria and accelerate the beam through the transition. We hope to attempt this in the near future.

\*Work supported by the Office of Naval Research.

### BEAM STABILITY

The circulating electron ring in the betatron possesses a number of types of modes of oscillation which can be driven unstable through interacting with each other or with a resistive wall or with gaps in the walls of the device, etc. Here, we consider only the first type of instability, which includes the well-known negative mass instability.<sup>9</sup> To obtain an analytic dispersion relation, we model the beam as a ring which can displace rigidly in the transverse direction and which can compress in the toroidal direction. The field equation used is that for the  $m=0$ , ( $m$  = poloidal mode number) perturbed toroidal electric field  $E_\theta^{(1)} \exp(i\ell\theta - i\omega t)$ ,

$$\nabla_\perp^2 E_\theta^{(1)} \approx 4\pi i \left( \frac{\ell}{R} \rho^{(1)} - \omega J_\theta^{(1)} \right) \quad (1)$$

where  $\ell$  is the toroidal mode-number,  $R$  is the major radius of the torus and  $\rho^{(1)}$  and  $J_\theta^{(1)}$  are the perturbed charge and current densities. Equation (1) drops toroidal corrections to the field equation and assumes  $|\ell/R| \approx |\omega| \ll 2\pi/a$ , where  $a$  is the minor radius of the torus. In this model, toroidal effects enter only in computing the  $m=0$  component of the charge density  $\rho$  which satisfies

$$\frac{\partial \rho}{\partial t} + \rho \frac{V_r}{r} + \frac{\partial}{\partial \theta} \left( \rho \frac{V_\theta}{r} \right) = 0 \quad (2)$$

where  $r(\theta)$  is the radial location of the beam centroid and  $V_r$ ,  $V_\theta$  are the beam velocity components. Equation (2) shows that rigid transverse ( $m=1$ ) displacements contribute to the perturbed net ( $m=0$ ) charge density. This coupling leads to the negative mass instability and other instabilities. To relate  $\rho^{(1)}$ ,  $V_\theta^{(1)}$ ,  $V_r^{(1)}$  to  $E_\theta^{(1)}$  we use equations similar to those of Sprangle and Vomvoridis.<sup>10</sup> Solving Eq. (1) we obtain the dispersion relation

$$1 = \frac{\omega_b^2 r_b^2}{4} (1 + 2\ell n a/r_b) \left\{ \frac{\ell}{\gamma \Delta \omega^2 R^2} \left( 1 - \frac{\omega^2 R^2}{\ell^2} \right) \left( \frac{\ell}{\gamma^2} - \frac{\omega \Omega_z / \gamma (\omega_0^2 - \Delta \omega^2)}{D} \right) - \frac{\omega^2 \Omega_z / \gamma}{\ell D \gamma \Delta \omega} \left( \omega_0^2 - \Delta \omega^2 \right) \right\} \quad (3)$$

where  $\omega_b^2 = 4\pi n_0 e^2/m$ ,  $n_0$  is the beam density  $r_b$  is the beam radius,  $\Delta \omega = \omega - \ell \Omega_z / \gamma$ ,  $\Omega_z = eB_z/mc$ ,  $\omega_0^2 = 1/2(1 - \omega_b^2 r_b^2 / \gamma \Omega_z^2 a^2) \Omega_z^2 / \gamma^2$ ,  $D = (\Delta \omega^2 - \omega_0^2)^2 - \Delta \omega^2 \Omega_\theta^2 / \gamma^2$ ,  $\Omega_\theta = eB_\theta/mc$ , where  $B_\theta$  is the toroidal magnetic field. Equation (3) differs from the dispersion relation in Ref. 10 in that the approximation  $\omega \approx \ell \Omega_z / \gamma$  has not been made (as well as in other more minor respects). This results in growth rates from two to ten times larger than those obtained in Ref. 10, as shown in Fig. 2. A more detailed discussion of Eq. (3) is given in Ref. 11.

The model used to derive Eq. (3) assumes that the beam is cold, and neglects finite  $v/\gamma$  ( $v$  = Budker's parameter) corrections to the vertical magnetic field and external field index, which can be fairly large.<sup>12</sup> A model without these assumptions

would be difficult to treat analytically, so we have resorted to 3-D particle simulations using IVORY (the instabilities in question are 3-D in nature). This has the advantage of allowing us to follow the non-linear development of the instability. The minor cross-section of the torus is represented by a spatial grid, while the toroidal direction is treated as a sum of Fourier modes. To date, we have run just one case, with  $\gamma_0 = 14$ ,  $I = 10$  kA,  $R = 1$  m,  $r_b = 2$  cm,  $B_\theta = 1$  kG. The minor cross-section is a 20 cm  $\times$  20 cm square. The growth rate of the  $\ell = 1$  instability predicted from Eq. (3) is  $3.6 \times 10^7$  sec<sup>-1</sup>. The simulation shows a growth rate of about half this viz.  $1.6 \times 10^7$  sec<sup>-1</sup>. This reduction is probably due to the 5% spread in  $\gamma$  as a result of the variation of the electrostatic potential across the beam. Sprangle and Vomvoridis<sup>10</sup> compute that an energy spread  $\Delta \gamma$  should decrease the growth rate by an amount  $\ell \Delta \gamma c |\gamma^{-2} - (1/2 - n_s)^{-1}| / \gamma R = 2.1 \times 10^7$  sec<sup>-1</sup>, which agrees quite well with the simulation.

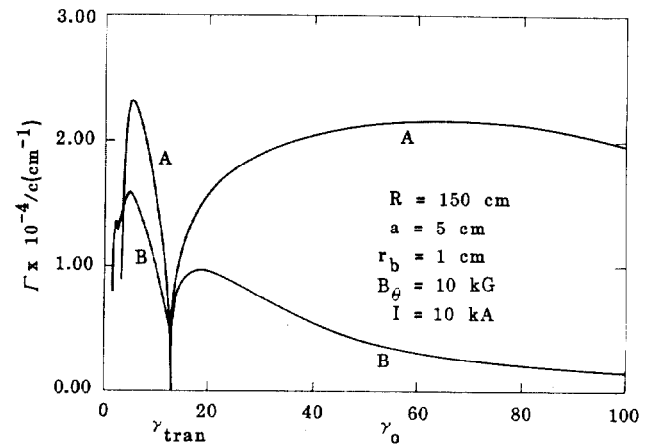


Figure 2. Comparison between growth rates obtained from Eq. (3) (Curve A) and those obtained from the dispersion relation in Ref. 10 (Curve B), for the  $\ell=1$  instability  $\gamma_{tran}$  occurs when  $\omega_\theta^2 = 0$ .

The beam is represented in IVORY by three separate groups of particles to resolve the  $\ell=0$  and 1 dynamics. During the linear stage of the instability, the three groups are equally spaced in  $\theta$  and almost identical, as seen in Fig. 3(a). As the instability develops into the nonlinear regime however, it produces noticeable kinking and longitudinal bunching of the beam, as seen in Fig. 3(b). In addition the beam heats up in both the transverse and longitudinal directions, which tends to decrease the growth rate significantly. However, the increased temperature causes the beam to develop "spiral arms" stretching out to the walls, causing loss of particles. At the point reached in Fig. 3(b), just 4% of the particles have been lost. This simulation will be run out further to determine if significant further losses will occur. In the near future, we intend to look at the effect of starting with a larger spread in energy on the beam.

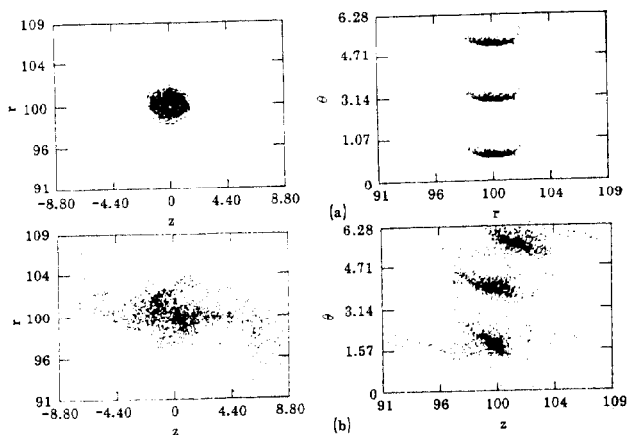


Figure 3. Position-space plots of beam during the (a) linear and (b) nonlinear stages of the instability. In the left-hand plots, particles at all  $\theta$ -positions are plotted. Dimensions are in cm.

#### REFERENCES

1. P. Sprangle and C. A. Kapetanacos, *J. Appl. Phys.* **49**, 1 (1978).
2. N. Rostoker, *Bull. Am. Phys. Soc.* **26**, 161 (1980).
3. D. W. Kerst, et. al., *Rev. Sci. Inst.* **21**, 462 (1950).
4. M. M. Campbell, B. B. Godfrey, and D. J. Sullivan, AMRC-R-454 (Mission Research Corporation, Albuquerque, 1983).
5. C. A. Kapetanacos, P. Sprangle and S. J. Marsh, *Phys. Rev. Lett.* **49**, 741 (1982).
6. H. S. Uhm and R. C. Davidson, *Phys. Fluids* **25**, 2334 (1982).
7. J. M. Finn and W. M. Manheimer, *Bull. Am. Phys. Soc.* **27**, 1131 (1982).
8. J. M. Finn, private communication.
9. R. W. Landau and V. K. Neil, *Phys. Fluids* **9**, 2412 (1966).
10. P. Sprangle and J. L. Vomvoridis, Naval Research Laboratory Memorandum No. 4688 (1982).
11. T. P. Hughes and B. B. Godfrey, AMRC-R-354 (Mission Research Corporation, Albuquerque, 1982).
12. P. Sprangle, C. A. Kapetanacos, and S. J. Marsh, 4th Conf. Electron and Ion Beam Research and Technology (Palaiseau, 1981).